Applied Catalysis B: Environment and Energy 348 (2024) 123841

Contents lists available at ScienceDirect

Applied Catalysis B: Environment and Energy

journal homepage: www.elsevier.com/locate/apcatb

In situ self-derived Co/CoO_x active sites from Co-TCPP for the efficient hydrogenolysis of furfuryl alcohol to 1,5-pentanediol

Taisan Xiang [a], Dengfeng Dai [a], Xin Li [a], Dandan Liu [a,*], Chao Feng [b,**], Pengcheng Dai [a], Liangjun Li [a], Xin Gu [a], Yunqi Liu [a,*]

[a] State Key Laboratory of Heavy Oil Processing, College of New Energy, College of Chemistry and Chemical Engineering, China University of Petroleum (East China), Qingdao, China

[b] Key Laboratory of Biofuels, Qingdao Institute of Bioenergy and Bioprocess Technology, Chinese Academy of Sciences, Qingdao 266101, China

ARTICLE INFO

Keywords:
Furfuryl alcohol
1,5-pentanediol
Metal-organic frameworks
Dual O adsorption
Oxygen vacancy

ABSTRACT

Revealing the mechanism for effective furan ring-opening process on transitional metal catalyst is critical for realizing the production of 1,5-pentanediol (1,5-PeO) through furfural alcohol (FOL). Herein, a Co-CoO_x metal-metal oxide catalyst derived from 2D Co-MOF was synthesized, exhibiting high selectivity for 1,5-PeO (46%) and suppressing the selectivity of 1,2-PeO to 3.74% at 170 °C, 3 MPa H_2 for 1.5 h. The coordination between Co^{2+} and ligand in MOF could form highly dispersed Co nanoparticles associated with CoO_x containing oxygen vacancy, and the inherited flower-like 2D nanosheets exposed more accessible Co-CoO_x active sites. Due to the proximity and synergistic effect between Co^0 and oxygen vacancy in CoO_x, the catalyst also realized the ring-opening of 2-methylfuran, and a mechanism based on dual O adsorption was proposed. This work demonstrates the decisive effect of oxygen vacancy during the formation of 1,5-PeO through FOL route, and deepen the understanding the mechanism of transition metal catalysts.

1. Introduction

To develop the sustainable chemical utilization of abundant energetic biomass, the conversion of biomass and platform compounds to value-added biofuels and chemicals has attracted public attention, which is a promising solution to the urgent demand of fossil resource alternative [1,2]. Furfural (FFA) is an important and economically produced bio-based chemical platform compound, which could transform into versatile high-value fuels and fine chemicals through hydrogenation [3] (Scheme 1a). 1,5-pentanediol (1,5-PeO) is the ring opening product of FFA through the cleavage of C-O-C bond and the hydrogenation of C═C bond in furan ring, and this valuable chemical could act as a monomer for the synthesis of polyesters and polyurethanes, or the ingredient for printing ink [4]. However, various hydrogenation routes are competitive with the ring opening of FFA. For example, the saturation of the C═C bond in the furan ring produces tetrahydrofurfuryl alcohol (THFA) [5], or the hydrogenation of C═O and subsequent hydrogenolysis of C-OH result in the formation of 2-methylfuran (2-MF) [6]. Besides, due to the existence and steric hindrance of C═O in FFA, the cleavage of the C-O-C bond in the furan ring still has two routes; only the cleavage of C_2-O_1 bond could form 1,5-PeO, while the breakage of C_5-O_1 bond is preferential because away from hindrance [7]. Therefore, to enhance the preferential cleavage of C_2-O_1 during the hydrogenation reactions, catalyst is the crucial key for this challenge.

Much effort has been devoted to developing catalysts for realizing the conversion of FFA and its derivatives, FOL and THFA, to 1,5-PeO by hydrogenation reaction through a one-pot process (Table S1). The noble catalyst with M-M'O_x (M: Rh, Ir, and Pt *et al.*, M'O_x: ReO_x, MoO_x, and WO_x *et al.*) sites could realize the hydrogenation of FFA to 1,5-PeO with high yield (50–70%) through THFA route. However, as the ring opening of saturated furan ring in THFA requires higher energy [8], the reaction has to achieved under high H_2 pressure (6–8 Mpa), low ratio of reactants and catalysts, and long reaction time (≥ 20 h) [9–11]. The ring-opening process was achieved by the adsorption of -OH on the M'O_x site and the attack of H^- formed by heterolytic cleavage on the metal site. The transition metal catalysts could also achieve the hydrogenolysis of the furan ring through FOL as a reaction intermediate. Zhao [12] et al. designed Cu-based core-shell Cu@MgO-La_2O_3 catalysts to realize the

* Correspondence to: State Key Laboratory of Heavy Oil Processing, College of New Energy, China University of Petroleum (East China), Qingdao, China.
** Corresponding author.
E-mail addresses: liudandan@upc.edu.cn (D. Liu), fengchao@qibebt.ac.cn (C. Feng), liuyq@upc.edu.cn (Y. Liu).

https://doi.org/10.1016/j.apcatb.2024.123841
Received 18 December 2023; Received in revised form 3 February 2024; Accepted 12 February 2024
Available online 13 February 2024

hydrogenolysis of furan ring and suppress the hydrogenation of FOL, in which the alkaline metal oxides, MgO and LaO, anchored C-OH in FOL and the Cu^0 sites realized the ring-open of furan ring. However, the selectivity of 1,2-PeO (63.7%) was superior to 1,5-PeO (18.8%). The other Cu-base catalysts, such as Cu-Al_2O_3 and Cu-$Mg_3AlO_{4.5}$ catalysts, draw similar conclusion that the cleavage of C_5-O_1 in hydrogenolysis of furan ring is preferential on Cu-based catalysts [13]. Shogo Shimazu[14] et al. reported a 42% selectivity of 1,5-PeO and 1.3% selectivity of 1, 2-PeO from Ni-based Ni-Y_2O_3 catalyst at 150 °C, 2 MPa H_2 and 24 h, but Ni is an excellent candidate for the hydrogenation of FOL to THFA. The high selectivity for THFA (30.4%) and the modest reaction efficiency still needs improvement. The Co-based catalysts are also effective for this catalytic system. Shao[15] et al. synthesized Co-Mg-Al catalysts from layered double hydroxides, which realize the conversion of FOL to 1,5-PeO (35.0% yield) at 140 °C and 4 MPa H_2 for 8 h in ethanol; Jaehoon Kim[16] et al. converted FOL to 1,5-PeO (47.5% yield) over Ni-CoO_x-Al_2O_3 trimetallic catalysts at 160 °C and 3 MPa H_2 for 6 h in ethanol; Ding[17] et al. report the direct FOL conversion to 1,5-PeO by Ni-Co-Al trimetallic catalysts, and the selectivity of 1,5-PeO (42.5%) exceed 1,2-PeO (12.2%) significantly. Accordingly, the Co-based catalyst has the potential to realize the direct hydrogenolysis of FOL to 1, 5-PeO. Although the Co-based catalytic system could achieve enhanced performance, the microscopic reaction mechanism is ambiguous. Besides, the Co-based catalysts with multimetallic component are mainly synthesized by hydrotalcite or coprecipitation method, which barriers the precise regulation of micro-structure. In addition, the sparse porosity of the Co-based catalyst limits the rate of mass transfer during the reaction, and determining the precise role of specific component in catalyst is challenging. Metallic Co^0 is the hydrogenation site, while the effect of oxide was indistinct because of its complexity, multifunction, and multi-component characteristics. The oxide is both support and adsorption sites, and the arrangement of different oxides and Co^0 sites is disordered, which bring difficulty to understand the proximity effect between the adsorption and hydrogenation sites in depth. Hence, designing a simple catalytic system with specific active sites is essential for revealing the mechanism and improving the reaction efficiency for directly converting FOL to 1,5-PeO.

Co-based metal-organic frameworks (MOFs) are ideal precursors for designing Co-based catalysts with homogeneous active sites [18]. The crystal structure of MOF precursor is well-defined and easy-modulated, therefore the uniform Co clusters could convert to specific Co-based active sites. The organic ligands could not only restrict the aggregation of Co-based active sites, but also transform into carbon-based support without adsorption sites. Besides, monometallic catalytic system can identify the hydrogenation sites and adsorption sites specifically, and the abundant porous structure in MOF could be inherited in the derivative materials, which is helpful to overcome the limitation of mass transfer and enhance reaction efficiency. Therefore, the derivatives of Co-based MOFs afford a strategy for cognizing the nature of conversion from FOL to 1,5-PeO.

Herein, a strategy was proposed to synthesize a model Co-based catalyst through Co-MOF for verifying the chemical process and proximity effect of functional sites in the hydrogenolysis of FOL to 1,5-PeO. In detail, a series of carbon-supported Co-CoO_x catalysts with different Co-CoO_x ratios were prepared by pyrolyzing of Co-TCPP (assembled by 2D nanosheets). The 2D lamellar structure could enhance the exposure ratio of accessible active sites and facilitate mass transfer, and the monometallic catalytic system could exclude the possible synergy of other metal oxides, which is an ideal model catalyst for studying the mechanism of transition metal catalyst. The optimized catalyst could achieve superior productivity of 1,5-PeO (15.2 $mmol \bullet g_{cat}^{-1} \bullet h^{-1}$), and present a distinct selectivity difference between 1,5-PeO (46.0%) and 1,2-PeO (3.7%). Transmission electron microscopy (TEM), X-ray photoelectron spectroscopy (XPS), electron paramagnetic resonance (EPR), and density functional theory (DFT) calculations confirm that the superior catalytic performance is attributed to the CoO_x decorated with oxygen vacancies. It not only promotes the adsorption of FOL but also activates the C_2-O_1 bond in the furan ring. The optimized catalyst exhibits excellent catalytic stability and hydrogenolysis performance for other biomass-derived furan derivatives. The mechanism was proposed

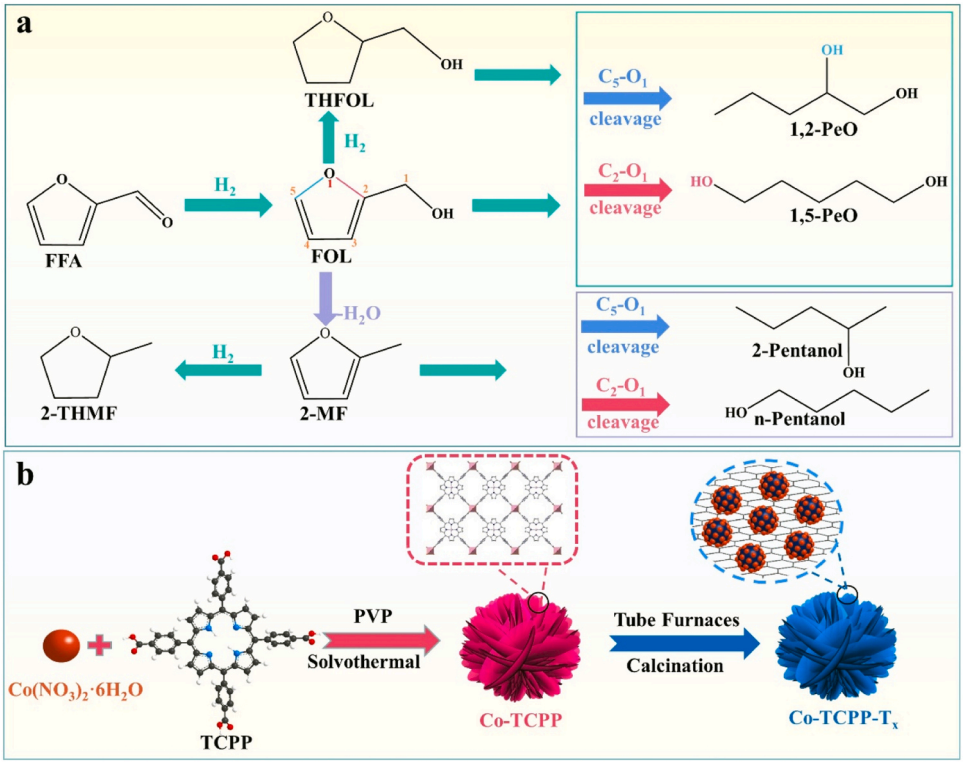

Scheme 1. a) Reaction pathways of furfural hydrogenation to derivatives. b) Synthesis route of Co-CoO_x/NCs from Co-TCPP.

based on in-situ DRIFT and density functional theory (DFT) results. This study will inspire the design of efficient transition metal catalysts to promote the preparation of renewable bio-based chemicals.

2. Experimental section

2.1. Materials

Cobalt nitrate hexahydrate ($Co(NO_3)_2{\cdot}6\,H_2O$, 99% purity), polyvinyl-pyrrolidone (PVP, MW=40,000 g·mol^{-1}), tetrakis (4-carboxyphenyl) porphyrin (TCPP, 97%), cobalt(II) tetraphenylporphyrin (Co-TPP), furfuryl alcohol (FOL), tetrahydrofurfuryl alcohol (THFA), 1,5-pentanediol (1,5-PeO), 1,2-pentanediol (1,2-PeO), 2-methylfuran (2-MF), 5-hydroxymethyl furfural (5-HMF) were obtained from Shanghai Aladdin Biochemical Technology Co., Ltd. N,N-dimethylformamide (DMF, 99.8%), n-pentanol, 2-pentanol, ethanol (99.9%), methanol (99.9%), isopropanol (99.9%) were purchased from Sinopharm Chemical Reagent Co., Ltd (China). All chemicals were used as received without further purification.

2.2. Preparation of catalysts

2.2.1. Synthesis of Co-TCPP MOF precursor

Typically, $Co(NO_3)_2{\cdot}6\,H_2O$ (1.6 mmol, 0.466 g) and polyvinylpyrrolidone (PVP, 0.08 g) were dissolved in 64 mL mixed solvent (3:1, [DMF: ethanol, v/v]), and then stirred magnetically until forming homogenous solution. Subsequently, TCPP (0.048 g) was added to the above solution, and stirred for 30 min. The obtained transparent solution was transferred into 100 mL Teflon-lined stainless-steel autoclave and kept at 80 °C for 24 h. After cooling to room temperature, the product was separated by centrifugation, washed with ethanol, and dried in an oven at 60 °C for 12 h to obtain the purplish-red MOF precursor, labelled as Co-TCPP.

2.2.2. Synthesis of Co-TCPP-T $_x$

The as-prepared Co-TCPP precursor was calcined at certain temperature (350, 400, 450, 500, 550, 600 °C) for 4 h under flowing H_2/Ar (10/90, v/v) in a tube furnace with a heating rate of 5 °C· min^{-1}. After cooling to room temperature, the resulting reduction products were marked T_{350}, T_{400}, T_{450}, T_{500}, $T_{550,}$ T_{600}.

2.3. Catalytic activity evaluation

The catalytic reactions were performed in a stainless-steel batch reactor (100 mL) equipped with a mechanical agitator. For a typical conversion, 50 mg of catalyst, 250 mg of reactant, and 50 mL of ethanol solution were added to the reactor. The autoclave was purged four times with H_2 (99.999%) to remove the air and charged with a certain H_2 pressure (1–4 Mpa). Then, the autoclave was heated to the specified temperature (120–180 °C) upon stirring at 800 rpm for a short time, and the reaction was performed for varying times (1–3 h). The liquid samples (0.25 mL) were withdrawn at the stipulated time during the reaction as needed. After the completion of reaction, the autoclave was quenched with cold water immediately. The liquid samples were separated from the catalyst by centrifugation and were qualitatively analysis using gas chromatography (GC, Fuli). The targeting products were identified by the available standards and GC-MS, and the quantitative analyzing of targeting products was performed by the area normalization method (corrected by the response factors of the standard chemicals). The conversion of reactant and the selectivity of each targeting product was calculated using the following equation:

$$\text{Conversion}(\%) = \left(1 - \frac{\text{Moles of FFA after reaction}}{\text{Initial moles of FFA}}\right) \times 100\% \quad (1)$$

$$\text{Selectivity}(\%) = \frac{\text{Moles of one product}}{\text{Total moles of FFA converted}} \times 100\% \quad (2)$$

$$\text{Yield}(\%) = \frac{\text{Moles of product}}{\text{Moles of initial FFA}} \times 100\% \quad (3)$$

2.4. Catalyst characterizations

The phase and crystallinity of catalysts were analyzed by Panalytical X'Pert PRO MPD X-ray diffractometer (XRD) using Cu Kα radiation (scan angle: 5–75°; scan speed: 0.2°·s^{-1}). The morphology of catalysts was observed using a Zeiss Genimi 300 thermal field-emission scanning electron microscope (FE-SEM) operating at 3 kV. Transmission electron microscopy (TEM) was used to analyze the microstructure of the catalyst by JEOL JEM-2100 (UHR) instrument. The textural properties of the sample were characterized by N_2 adsorption-desorption isotherms on Quantachrome Autosorb-iQ volumetric adsorption apparatus at 77 K. The changes in chemical environments were monitored by a Thermo Scientific ESCALAB 250Xi X-ray photoelectron spectrometer (XPS), and the XPS peaks were calibrated with reference to the C1s peak at 284.8 eV. The oxygen defects was tested by electron paramagnetic resonance (EPR) using Bruker EMX plus, Germany. The thermal decomposition process was investigated by thermal gravimetric (TG) analysis using STA449F5 apparatus in Ar atmosphere with a heating rate at 10 °C·min^{-1}. Fourier transform infrared spectra (FT-IR) were performed on a Bruker 4700 FT-IR spectrometer by potassium bromide pressed disk.

The temperature-programmed desorption of ammonia (NH_3-TPD), hydrogen (H_2-TPD), and H_2 pulse chemisorption were carried out on a Builder PCA-1200 chemisorption analyzer. Before the NH_3-TPD test, the sample was pretreated at 200 °C for 2 h in Ar (30 mL·min^{-1}), then the sample was purged with NH_3 (40 mL·min^{-1}) at 80 °C for 40 min until the surface was saturated by NH_3. Subsequently, the NH_3 by physisorption was purged by flowing Ar until the baseline was stable. The desorption proceeded from 80 to 500 °C at 10 °C/min in Ar and maintained at 500 °C until the TCD signal returned to baseline, and the signal at m/z=17 (NH_3) was recorded by mass spectrometry to avoid interference by sample decomposition.

For the H_2-TPD, the sample was pre-treated by H_2/Ar (10/90, v/v, 40 mL·min^{-1}) flow at 300 °C for 100 min. The sample was naturally cooled to 50 °C under H_2/Ar flow and kept at 50 °C for another 30 min. Then, the sample was purged with Ar (30 mL·min^{-1}) for 30 min to remove physical adsorbed H_2 molecules until the baseline was stable. The H_2-TPD analysis was performed from 50 °C to 300 °C at 10 °C/min under Ar flow. The desorbed gas was detected by the TCD detector.

H_2 pulse chemisorption was used to analyze the dispersion of the Co-active center (D_{Co}) and the active specific surface area (S_{Co}). Based on the above results, the turnover frequency (TOF) of the catalyst could be determined. For the H_2 pulse chemisorption, the sample was reduced under H_2/Ar (10/90, v/v, 40 mL·min^{-1}) flow at 300 °C for 100 min, then purged with Ar (30 mL·min^{-1}) at 300 °C for 1 h and cooled to 50 °C. Subsequently, a 10% H_2/Ar pulse was injected into the reduced catalyst bed using Ar as a carrier gas at 50 °C. Pulses were introduced by a calibrated sample loop (V_{loop} = 0.2 mL). The adsorbed amount of H_2 and resulting Co dispersion were calculated from the number and area of the adsorbed pulses and following equations.

$$\boldsymbol{n}_{H_2} = \frac{\text{NA1} - \text{A2}}{\text{A1}} \times \frac{V}{V_m} \quad (4)$$

$$\mathbf{D}_{\mathbf{Co}} = \frac{\text{n}_{H_2} \times \text{M}_{\text{Co}} \times \text{z}}{\text{m}_{\text{c}} \times \text{w}} \quad (5)$$

Here, n_{H2} is the moles of H_2 consumed by catalyst, N is number of pulses injected, A1 is the area when empty tube is injected with pulse, A2 is the total area at pulse saturation, V is the volume of sample loops, V_m is the molar volume of gas, M_{Co} is the relative atomic mass (58.9 g/

mol), m_c is the mass of catalyst, w is the mass fraction of active metal in the catalyst, the value of z was 2 considering the dissociative chemisorption of H_2 on Co.

For calculating the turn over frequency (TOF) of catalysts, the FOL conversion was kept below 30%.

$$\mathrm{TOF}\left(h^{-1}\right) = \frac{\text{Moles of reactant converted}}{\text{Moles of metal Co on the surface of catalyst} \times \text{Reaction time}} \quad (6)$$

In situ diffuse reflectance infrared Fourier transform spectroscopy (DRIFT) was conducted by Bruker VERTEX70 spectrometer to reveal the FOL hydrogenation process. The catalyst loaded in an in-situ transmission cell was first reduced at 450 °C for 1 h by H_2/Ar (10/90, v/v), and cooled to room temperature. The reactant FOL was introduced on the surface of the sample, and Ar was purged to remove the physically adsorbed FOL, then a spectrum was collected as background. Subsequently, the temperature of the cell was programmed from 30 to 170 °C, and the spectra for the hydrogenation process of FOL were collected at a certain temperature with the introduction of H_2/Ar simultaneously.

3. Results and discussion

3.1. Catalyst characterization

The synthesis route of Co-CoO_x/NCs is illustrated in Scheme 1b. As shown in Figure S1, the XRD pattern of Co-TCPP displayed a characteristic diffraction peak at 7.5°[19]. With the thermal treatment in hydrogenous atmosphere, the reduction process resulted in structural transformation from MOF precursor to Co-CoO_x/NCs samples (Fig. 1a). When the temperature was below 500 °C, the diffraction peaks associated with MOF and Co species were not detected, indicating the formation of Co species with high dispersion. After the temperature was raised to above 550 °C, samples showed characteristic reflections at 44.4° and 51.7°, which indexed to (111) and (200) crystal plane in Co phase (JCPDS: 15–0806). Further increasing the treatment temperature, the intensities of diffraction peaks at 44.4° and 51.7° were strengthened, indicating the aggregation of Co particles. Besides, the new peak detected at 26.1° in T_{600}, was attributing to the C (002) crystal plane (JCPDS: 50–1083), and its formation was due to the enhanced carbonization degree of the ligand. The results implied that the frameworks of Co-TCPP materials was decomposed, and new Co species and carbon materials were generated during the calcination process. This conclusion was confirmed by FT-IR. As shown in Fig. 1b, the stretching vibrational of C═O and C-OH located at 1693 cm^{-1} and 1401 cm^{-1} were originated from carboxylate group in ligand TCPP [20], and those bands shifted to 1659 and 1391 cm^{-1} after coordinating with the Co^{2+}. The vibration of N–H bonds in pyrrole rings at 968 cm^{-1} was replaced by a new peak at 1005 cm^{-1}, indicating the Co^{2+} was immobilized through Co-N bond [21]. After calcining at 350 and 400 °C, the peaks attributing to carboxylate group disappeared, but the Co-N bond still existed after calcination at 400 °C, suggesting that the decarboxylated reaction occurred and the porphyrin ring structures maintained. As expected, new peaks at 576 and 663 cm^{-1} attributed to the Co-O stretching vibration were formed, indicating the formation of CoO_x after decarboxylation. When the temperature further increased to above 450 °C, the bands attributing to Co-N and Co-O were both weakened, attributing to

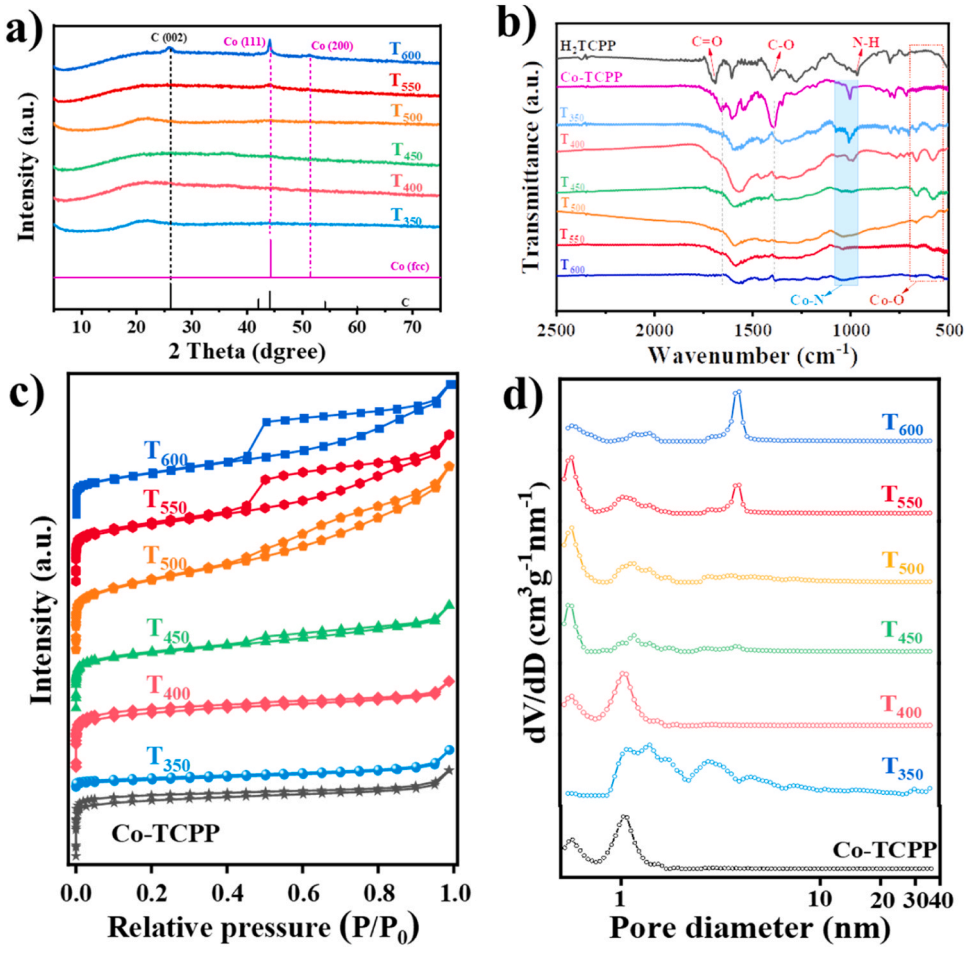

Fig. 1. a) XRD patterns of the Co-MOF derived samples calcined at different temperature. b) FT-IR spectra of organic ligands, Co-TCPP and calcined samples. c) N_2 adsorption-desorption isotherms and d) pore size distribution of samples before and after calcination.

the decomposition of porphyrin structures and the reduction of CoO_x. The evolution of textural structures in catalysts was investigated using N_2 adsorption-desorption isotherms (Fig. 1c). The Co-TCPP precursor exhibited type-I isotherms, indicating micropores were dominant in the frameworks. As the treatment temperature increased, the mesoporous surface area of samples increased and the micropores were sacrificed accordingly (Table S2). Besides, the hysteresis at P/P_0 in the range of 0.4–1.0 became prominent, indicating the decomposition of MOF resulted in a mesoporous structure. The BET surface area of treated sample could reach 300 $m^2 \cdot g^{-1}$, which was superior to the hydrotalcite-derived catalyst, favoring the mass transfer during the reaction. As displayed in Fig. 1d, the pore size distribution of samples was consistent with the above conclusion; the micropores in Co-TCPP concentrated in 1.1 nm were partially expanded to 4.1 nm after calcination.

The morphology of catalysts was further investigated via SEM (Fig. 2a). As shown in Fig. 2a1, the obtained Co-MOF precursor possessed flower-like microspherical morphology assembled by vertical-oriented nanosheets with 65 nm thickness, and the as-prepared catalysts inherited the flower-like skeleton from the Co-TCPP precursor after calcination. Furthermore, increasing the reduction temperature from 350 to 600 °C facilitated the decomposition of MOF and the carbonization of ligands, which results in porous, rough, and loose nanosheets with wrinkles (Fig. S2). Besides, as the degree of reducibility increased, the ultrafine nanoparticles could be observed on the wrinkled substrates. After the temperature increases to 600 °C (Fig. 2a4), the macromolecular ligand tended to aggregate into a carbon layer without the limitation of coordination. Different with MOF precursor, the TEM images of the calcined samples presented high density of cobaltic nanoparticles with uniform dispersion on nanosheets (Fig. 2b, Fig. S3). The average particle size is 1.5 nm for T350 and 2.2 nm for T_{450}, which is under the detection limit of XRD. The particles aggregated to 7.5 nm after the

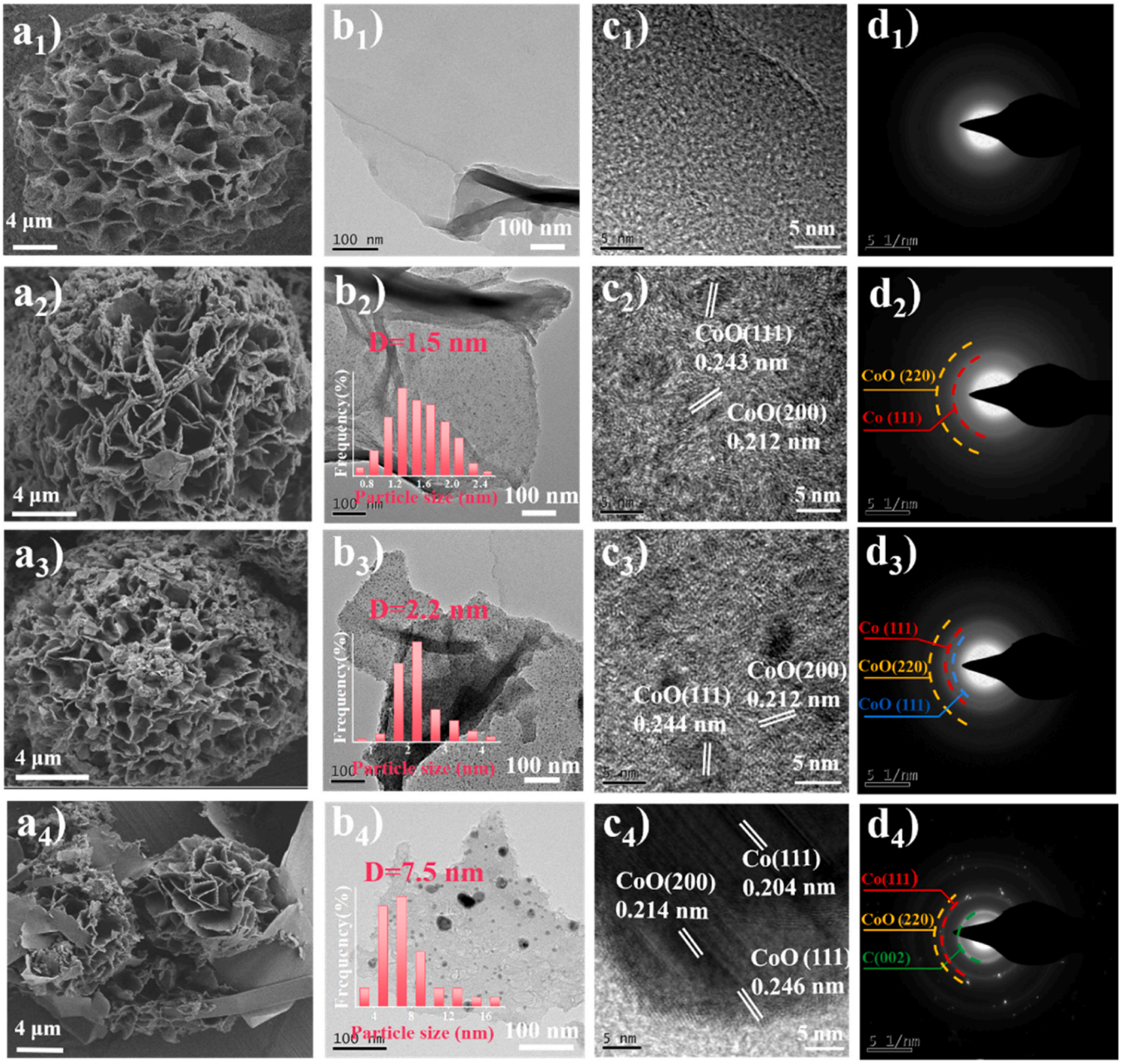

Fig. 2. a) SEM images, b) TEM images and Co nanoparticles size distributions, c) HR-TEM images and d) SAED images of 1) Co-MOF precursor, 2) T_{350}, 3) T_{450} and 4) T_{600} catalyst, respectively.

temperature reached 600 °C, and the main phase was metallic Co based on XRD results. HRTEM images displayed clear lattice fringes corresponding to Co (d_{111}=0.204 nm) and CoO (d_{200}=0.212 nm, d_{111}=0.244 nm), which is further confirmed by SAED (Fig. 2c, d). The lattice fringes of nanoparticles in catalyst obtained below 500 °C was mainly attributed to CoO_x, and the lattice fringes of Co^0 could be detected easily after the temperature reached 550 °C. The faint halos indicated the small dimension of corresponding phase, and the appearance of Co (111) diffraction ring implied the uniform nanoparticles consist of metallic Co and CoO_x had already formed under the treatment at 350 °C. In addition, the SAED diagram of T_{600} catalyst (Fig. 2d4) presented the ring of C (002) crystal plane, evidencing the formed nanosheets is a carbon film.

3.2. Catalyst evaluation

The samples synthesized from Co-TCPP were used for evaluating the conversion of FOL under hydrogen, and the catalytic performance of derived catalysts was summarized in Table 1. The active sites of catalysts were modulated by varying the reduction temperature of Co-TCPP. When the reaction system was performed without a catalyst or using pristine Co-TCPP as the catalyst, the conversion of FOL was negligible. By using the catalyst obtained at 350 °C, the conversion of FOL could reach 80.3%, and 1,5-PeO is the main product. As the treatment temperature of catalyst increased from 400 to 500 °C, the conversion of FOL increased to 97%, and the selectivity of 1,5-PeO and 2-MF was slightly improved to 46% and 27%, whereas those of THFA decreased to 16.8% compared with T_{350}. In contrast, over the catalyst obtained at 550 and 600 °C, the FOL conversion and selectivity of 1,5-PeO decreased distinctly. Then, the optimized catalyst T_{450} was chosen to react under an inert atmosphere to exclude the intervention of catalytic hydrogen transfer. Even though using furfural as reaction substrate, the 1,5-PeO is still the main product, but the selectivity of THFA and 2-MF was improved due to the competitive reaction of furan ring hydrogenation and enhanced hydrogen consumption.

The reducing temperature determines the ratio of metallic Co and CoO_x in the active sites, and the distinct difference in catalytic performance has a close relationship with the intrinsic property of active sites. In this catalytic system, Co is the hydrogenation site, and the coordination unsaturated CoO_x acts as the adsorption sites, and the cooperation between them realizes an obvious distinction from 1,5-PeO to 1,2-PeO. The catalysts obtained between 400 and 500 °C corresponded to the decomposition process of MOF precursor (Fig. S4); therefore, T_{450} was selected as a representative to study the structure-performance relationship between catalysts.

Table 1
The catalytic performance of Co-TCPP and derived catalysts.

Sub.	Cat.	Conv. (%)	Sel. (%)				
			1,5-PeO	1,2-PeO	THFA	n-pentanol	2-MF and D
FOL	None	0.74	–	–	64.4	–	35.6
FOL	CoO	7.2	–	–	–	100.0	–
FOL	Co-TCPP	4.4	–	–	13.2	24.3	62.5
FOL	T_{350}	80.3	42.2	2.8	29.4	5.2	20.4
FOL	T_{400}	97.1	44.7	3.5	20.5	6.7	24.6
FOL	T_{450}	97.2	46.0	3.7	16.8	7.0	26.5
FOL	T_{500}	97.6	45.0	3.6	17.1	6.8	27.5
FOL	T_{550}	87.7	42.6	2.9	18.8	7.1	28.6
FOL	T_{600}	34.5	33.4	1.3	36.2	3.3	25.8
FOL	T^a_{450}	0.97	–	–	59.1	–	40.9
FFA	T_{450}	97.7	34.6	3.3	22.7	6.1	33.3

a: Reaction was performed under Ar atmosphere to exclude the catalytic hydrogen transfer reaction induced by ethanol; b: D means derivative from the hydrogenation of 2-MF; Reaction conditions: 50 mg catalyst, 50 mL ethanol solution with 250 mg furfuryl alcohol, stirring speed=800 rpm, T=170 °C, H_2 pressure=3 Mpa, t=1.5 h.

3.3. Optimization of reaction conditions

The catalytic conversion of FOL to 1,5-PeO is a pressure and temperature-dependent process, therefore the catalytic performance of T_{450} was evaluated at different reaction temperatures, H_2 pressure, and reaction time. 1,5-PeO is the major product with predominant selectivity under different reaction conditions. As shown in Fig. 3a, the conversion of FOL was 23.9% at 120 °C, and could reach 95% at 140–180 °C. The selectivity of 1,5-PeO was relatively stable at 140–180 °C (above 40%), while the 2-MF selectivity increased from 14.1% to 30.8% with the increased temperature, and the selectivity of THFA dropped accordingly. The T_{450} exhibited the highest selectivity of 1,5-PeO (45.1%) at 170 °C, and then the catalytic performance was declined due to the progressively enhanced formation of 2-MF at higher temperatures.

Then the effects of H_2 pressure on FOL conversion and products distribution were presented in Fig. 3b. The conversion of FOL was only 35% when the H_2 pressure was 1 MPa, and 2-MF were found to be the major products (selectivity 56.7%), indicating sufficient H_2 in the atmosphere is essential for the ring-opening process. As H_2 pressure increased, T_{450} presented the best performance ($S_{1,5\text{-PeO}}$: 44.5%) at 3 MPa, then the route to THFA was improved with enhanced H_2 pressure, resulting in the decrease of 1,5-PeO selectivity. Therefore, H_2 pressure is an important factor for the ring-opening reaction of FOL. The hydrogenolysis of furan ring could not realize at low hydrogen pressure, but excess hydrogen is beneficial for the hydrogenation of furan ring. Thus, 170 °C and 3 MPa H_2 pressure was chosen as the optimized reaction conditions for T_{450}.

To investigate the process of FOL conversion, the change of product with reaction time was monitored. As shown in Fig. 3c, the conversion of FOL was 64.9% at 0.5 h, then increased to above 90% at 1 h and remained steady thereafter. Furthermore, the stable product distribution indicated that the three reaction route (ring-opening, ring hydrogenation, hydrodeoxygenation) were performed simultaneously, and further confirmed that the origin of 1,5-PeO and 1,2-PeO was not from the ring-opening process of THFA.

To figure out whether the variation of mass ratio between the catalyst and FOL could affect the product distribution (Fig. 3d), the catalytic process over T_{450} under different $ratio_{(Catalyst/FOL)}$ was performed. The trend to form 1,5-PeO is enhanced under high $ratio_{(Catalyst/FOL)}$, while the formation of 2-MF was suppressed, and the reaction route to THFA was not affected. Therefore, it can be concluded that the competitive reaction route to 1,5-PeO was 2-MF, rather than THFA. As the $ratio_{(Catalyst/FOL)}$ decreased, more FOL was added in the reaction system. This led to an increased adsorption density of FOL on the catalyst surface and a tendency for vertical configuration due to space limitations. Additionally, since the unchanged initial H_2 pressure could not cover the consumption of FOL, the conversion of FOL to 2-MF by hydrodeoxygenation is more preferable. Hence, the selectivity of 2-MF was enhanced as more FOL was added. Considering the reaction efficiency, the mass ratio of 1:5 was chosen for further investigation.

Calculation of the productivity of 1,5-PeO under the optimized conditions showed that the T_{450} (15.2 $mmol \cdot g_{cat}^{-1} \cdot h^{-1}$) had a significant advantage over other catalysts (Fig. 3e). To correlate the catalytic behavior with the solvent, the hydrogenation reaction of FOL over T_{450} catalyst was performed in different solvents (Fig. 3f). When the catalyst was tested in methanol, 2-MF and its derivatives were the major species with 21% FOL conversion, and 1,5-PeO was not detected in the product. Different from the case in ethanol, both 1,5-PeO and THFA were the major products during the FOL conversion in isopropanol, suggesting that the provision of protons in isopropanol is favor for the hydrogenation saturation of the furan ring, rather than promoting the ring-opening reaction.

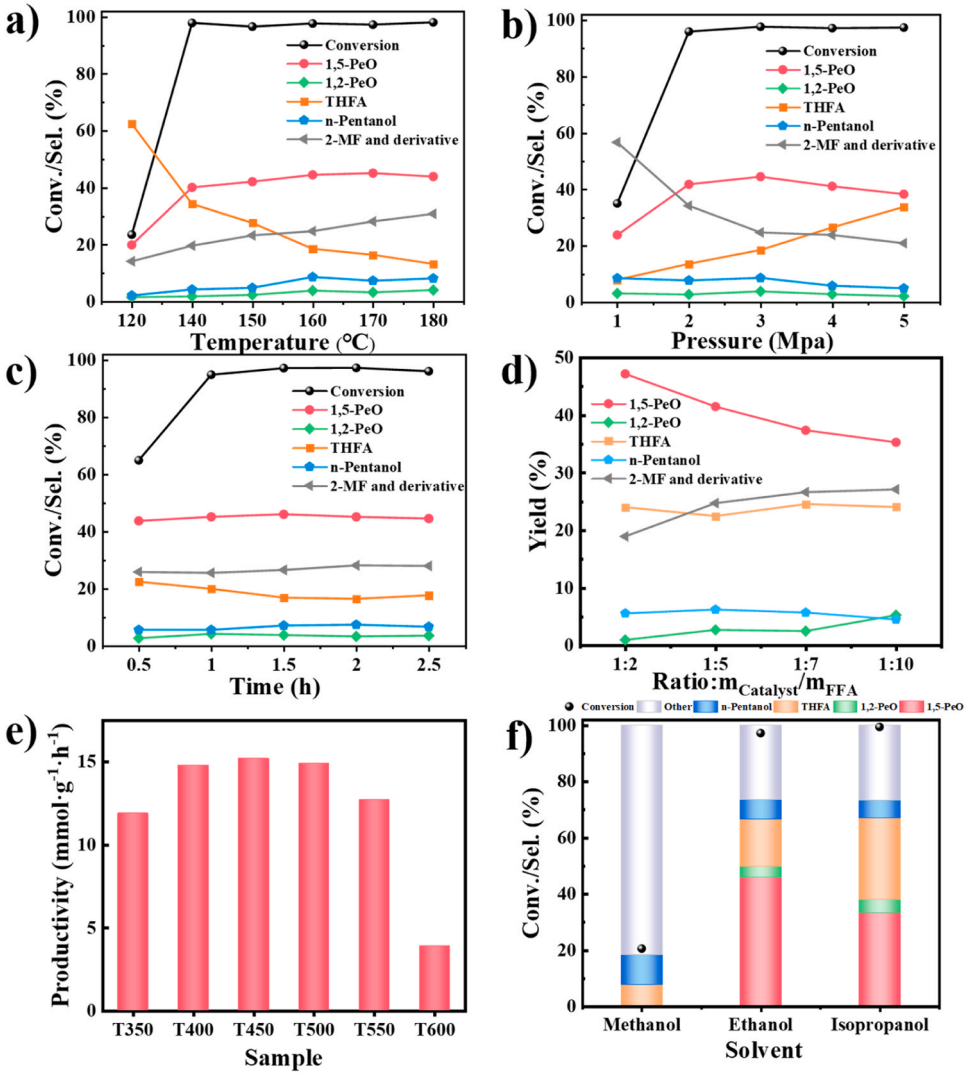

Fig. 3. FOL conversion and product selectivity of T_{450} catalyst at varying a) reaction temperature (reaction conditions: 3 Mpa H_2, 2 h), b) H_2 pressure (reaction conditions: 170 ℃, 2 h), c) reaction Time (reaction conditions: 170 ℃, 3 Mpa H_2), d) ratio: $m_{Catalyst}/m_{FOL}$ (reaction conditions:170 ℃, 3 Mpa H_2, 1.5 h), e) calcination temperature (reaction conditions:170 ℃, 3 Mpa H_2, 1.5 h), and f) solvent (reaction conditions: 170 ℃, 3 Mpa H_2, 1.5 h) by using 50 mg catalyst and 250 mg FOL in 50 mL ethanol solution.

3.4. Insight into the nature of active sites

To further elucidate the origin of active sites and the synergistic effect between adsorption sites and hydrogenation sites during the ring-open of the furan ring, we employed XPS, EPR measurements, and etching strategy to monitor the MOFs decomposition and composition of active sites. T_{350}, T_{450}, and T_{600} represent the different decomposition stages during the reaction and exhibit distinct catalytic performance, which are selected for further investigation.

To understand the chemical environments and existence form of Co species in the above catalysts, the XPS data were collected. The C 1 s spectrum of the Co-TCPP precursor was deconvoluted into five peaks at 284.6, 285.6, 286.6, 287.6, and 289.1 eV (Fig. S6), corresponding to C═C, C-C, C-N, C═N, -COO in the organic ligands [22]. The reduction temperature had little impact on the XPS spectra of carbon, only the ratio of peaks corresponding to C-N, C═N at 286.7 and 287.6 eV decreased obviously (Fig. 4a), demonstrating that the organic ligands were partially fractured after treatment at high temperature. The Co $2p_{3/2}$ spectra were deconvoluted by the Gaussian peak fitting method. For the Co-TCPP precursor, the two peaks at 782.5 eV and 780.4 eV corresponding to Co^{2+} $2p_{3/2}$ coordinated with carboxyl and Co-N_x $2p_{3/2}$ located within the porphyrin ring, with a satellite at 786.6 eV (Fig. S5) [23,24]. With the treatment at high temperatures, the peak attributing to Co^0 was appeared at 778.6 eV in Co $2p_{3/2}$ spectra, and the atom ratio of Co^0 increased from 5% to 19.5% (Fig. 4b). The weak peaks attributing to Co^{2+} further confirmed that Co^{2+} was partially reduced to metallic Co and the coexistence of Co^0 and Co^{2+}. The Co^{2+} ions coordinated with N were difficult to reduce [25], therefore, the ratio of Co-N_x is relatively stable during the treatment. The N 1 s spectra were deconvoluted into peaks at 398.6 eV for pyridinic-N, 399.2 eV for coordinated Co-N_x, 400.2 eV for pyrrolic-N, 401.1 eV for graphitic-N and 402.4 eV for pyridine-N oxide (Fig. S5, Fig. 4c), respectively [26,27]. The intensity of the graphitic-N peak increased with the raising of treatment temperature, mainly due to the improved graphitization. The O 1 s spectra of the catalysts (Fig. 4d) could be fitted into peaks at 529.9, 531.4, 532.2, and 533.8 eV, which attributed to lattice oxygen (O_L), oxygen vacancies (O_v), O-C/O-C═O groups (O_{C-O}) and surface hydroxyl functional groups (O_{O-H}), respectively [22]. The peaks of O_v and O_L appeared after treatment, indicating the formation of CoO_x with oxygen vacancies, and the slight shift of Oc-o after treatment was attributed to the transformation from carboxyl in ligands to oxygen functional groups on carbon support. Hence, the active sites on obtained catalysts contained metallic Co^0 sites,

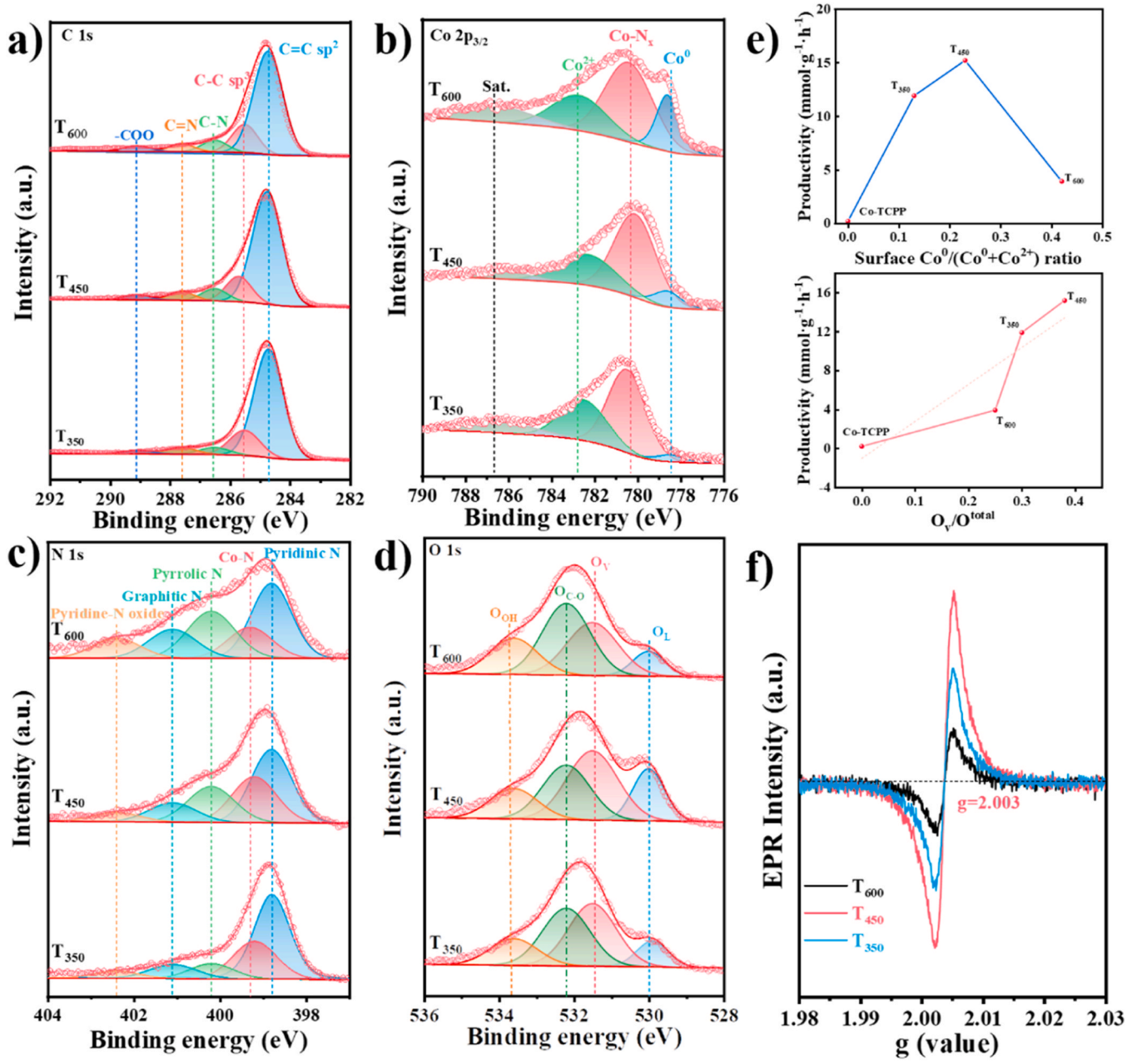

Fig. 4. a) C 1 s, b) Co $2p_{3/2}$, c) N 1 s, d) O 1 s XPS spectra, e) correlation of $Co^0/(Co^0+Co^{2+})$ and O_v/O^{total} with1,5-PeO productivity, and f) X-band EPR spectra of T_{350}, T_{450}, T_{600}.

coordinated Co-N species, and CoO_x phase with oxygen vacancies. Although hydrogenation is an important process during the formation of 1,5-PDO, the productivity presents a positive correlation with the amount of oxygen vacancies in catalysts, rather than the metallic Co^0 ratio on surface, indicating the adsorption of reactant molecules on the CoO_x sites is crucial for the ring-open process (Fig. 4e).

The electron paramagnetic resonance (EPR) spectra of obtained catalysts had a sharp and stronger resonance peak at g=2.003, which was typically considered to originate from the electron trap in oxygen vacancy. For the measured catalysts, T_{450} has higher oxygen vacancies than others (Fig. 4f), which is consistent with the catalytic performance for 1,5-PeO yields. It suggests that the suitable reduction treatment and

Table 2
XPS Data for the Co-TCPP and derivative prepared at different temperatures.

Sample	Atomic concentration (%)				Co^0		Co^{2+}		Co-N_x	
	C 1 s	N 1 s	O 1 s	Co 2p	B.E.	at%	B.E.	at%	B.E.	at%
Co-TCPP	76.6	7.6	13.1	2.7	–	–	782.6	40.0	780.6	60.0
T_{350}	82.8	6.6	7.4	3.2	778.4	5.0	782.5	34.4	780.5	60.6
T_{450}	80.7	6.0	9.5	3.8	778.6	9.1	782.7	31.1	780.5	59.8
T_{600}	90.9	3.0	4.7	1.5	778.6	19.5	782.7	27.3	780.5	53.2

the coordination in MOF precursor increased the concentration of oxygen vacancies in CoO_x, thereby improving the adsorption sites of FOL and enhancing the selectivity of 1,5-PeO [28]. Table 2

The amount and intensity of acid sites on catalysts were analyzed by NH_3-TPD, and the change of desorbed NH_3 molecules were recorded through QMS profiles, to eliminate the influence of other gases generated by the transition states of MOF on TCD signals. The T_{450} catalyst exhibited broad peaks centered at 348 and 383 °C, whereas the T_{350} and T_{600} catalysts only exhibited one negligible NH_3 desorption peak at 251 °C and 373 °C, respectively. The NH_3 desorption signals of T_{350} catalyst at 251 °C and T_{450} catalyst at 348 °C were related to the amount of weak Lewis acid sites of the metal Co^{2+} center in CoO_x; the signals at 383 °C for T_{450} catalyst and 373 °C for T_{600} catalyst originates from the coordination of NH_3 with electron deficiency in CoO_x (Fig. S7a)[16]. In general, the Co species in T_{350} sample reduced at 350 °C mainly existed as metal nodes in MOF, while the high reduction ratio and the formation of graphitized carbon layers in T_{600} limited the formation of electron deficiency in CoO_x. The catalyst with adequate acid strength and amount was correlated with a specific treatment temperature.

H_2-TPD was performed to investigate the dissociative adsorption of H_2 on the surface of catalysts. The low-temperature desorption peaks at 110 and 118 °C are attributed to dissociative H_2 adsorption on exposed Co^0 sites [15,29]. The desorption peaks at 190 and 205 °C are ascribed to the bridge adsorption of hydrogen at Co-Co coordination. The T_{450} sample displays the strongest dissociative adsorption and bridge adsorption of H_2, indicating that the adjacent CoO_x species contributes to the activation of hydrogen as reported (Fig. S7b). The dispersion of the Co active center (D_{Co}) of T_{450} were characterized using pulsed chemisorption (Fig. S7c). As shown in Fig. S8 and Table S3, the increased reaction temperature from 150 to 170 ℃ could accelerated the hydrogen of FOL significantly, and the activation energy (Ea) of T_{450} was calculated via the Arrhenius law. The T_{450} catalyst presented Ea with 20.7 kJ/mol, and the TOF could reach 88.8 h^{-1} at 170 ℃, those parameters are both superior to the reported catalysts [12,30].

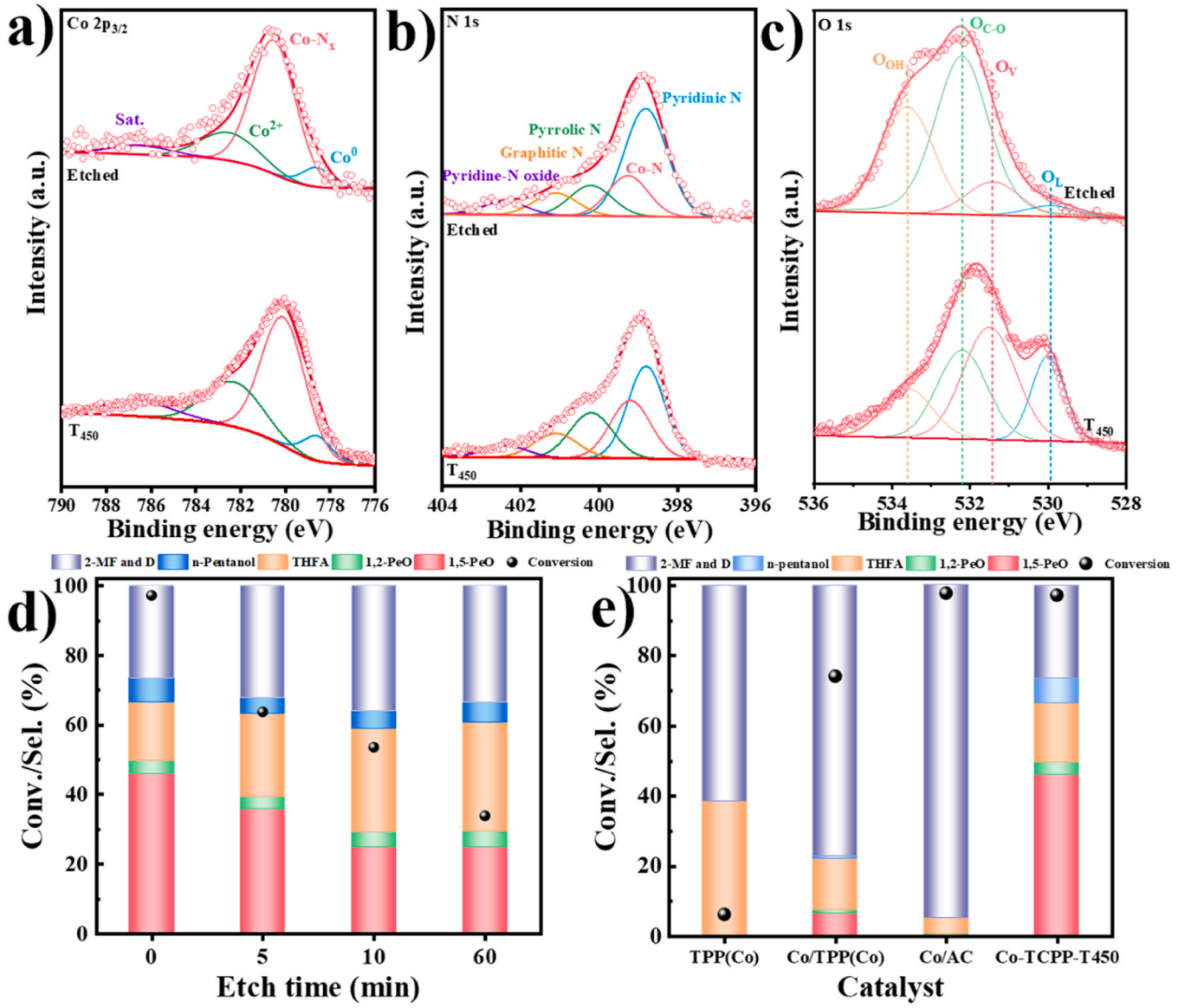

Fig. 5. a) Co $2p_{3/2}$, b) N 1 s, c) O 1 s XPS spectra of T_{450} catalyst before and after acid etching. d) FOL conversion and product selectivity of T_{450} catalyst etching in acid for different times. e) Catalytic performance of model catalysts derived from Co-TPP and impregnation. (50 mg catalyst, 50 mL of ethanol solution dissolved in 250 mg of FOL, 170 °C, 3 Mpa H_2, and 1.5 h.).

3.5. The role of CoO_x in the catalyst (discussion on structure-selectivity relationship)

Based on the catalytic results, the presence of CoO_x plays an important role in the ring-opening process. To distinguish the contribution of CoO_x and the synergistic effect of metallic Co and CoO_x in the catalyst, we utilized dilute acetic acid solution (10 wt%) to modulate the ratio of Co^0 and CoO_x, thereby synthesizing a series of univocal model catalysts with single variable. Before etching, we confirmed that the metallic Co could not react with dilute acetic acid solution (10 wt%) at room temperature, and only CoO could be removed during the etching process. Fig. 5a displays the Co $2p_{2/3}$ XPS spectra of T_{450} catalysts before and after etching, and XPS spectra of samples at different etching intervals are shown in Fig. S9. Notably, the peaks of Co^{2+} and the corresponding satellite located at 786.8 eV were suppressed gradually during etching, while the metallic Co^0, Co-N_x and N species were not affected (Figs. 5b, S9a), indicating that only CoO_x could be removed during the etching process. In addition, the significant decrease of O_L and O_v in the O 1 s profiles after etching further confirmed the removal of CoO_x (Figs. 5c, S9b), and the origin of O_v is mainly from CoO_x. Therefore, by prolonging etching times, the conversion of FOL decreased from 97.2% to 36.3% due to the reduced ratio of Co^{2+}. Additionally, there was a slight decrease in the selectivity of 1,5-PeO and an enhancement in the formation of THFA and 2-MF with the removal of O_v-CoO_x. (Fig. 5d). Thus, the removal of oxygen vacancies in the CoO_x phase could reduce the density of adsorption sites, resulting in the distinguished reduction of reaction efficiency. As the synergistic effect and proximity effect between Co and CoO_x were weakened during the etching process, the distribution of products was adjusted accordingly. This conclusion further confirmed that the CoO_x acts as the adsorption site during the reaction, and the adsorption of FOL on CoO_x could activate the furan ring and strengthen the ring-opening route.

To investigate the role of coordinated Co-N_x sites and oxygen vacancies, univocal model catalysts were synthesized based on cobalt tetraphenylporphyrin (TPP(Co)), in which Co^{2+} only existed in the form of Co-N_x coordination (Fig. S10a). Over the reduced TPP(Co)-R catalyst, the conversion of FOL was 6.2%, and most reactants proceeded through 2-MF and THFA pathway. Then Co^{2+} was introduced to TPP(Co) to recover the composition in Co-TCPP, and the reduced Co/TPP(Co)-R catalyst exhibited enhanced FOL conversion to 74%, but 2-MF and derivatives are still the major product. Besides, the diols could be detected. To eliminate the influence of TPP(Co), the reduced Co/AC catalyst by impregnating Co^{2+} on active carbon was synthesized. This catalyst presents high FOL conversion (97.8%) and 2-MF selectivity (>90%), and no ring-opening products were detected (Fig. 5e). These results indicate that the assistance of Co-N_x coordination during the ring-opening process of FOL is limited, and the effective active site mainly derived from the coordinated Co^{2+} with carboxylate. The Co species supported by impregnation possess weak metal-support interaction, and the enhanced reduction degree of Co^{2+}, as well as the decreased amount of oxygen vacancies in CoO_x are favorable for the hydrodeoxygenation reaction rather than the ring-opening pathway (Fig. S10b). Hence, the contiguous synergistic effect between Co and CoO_x with oxygen vacancies is crucial for the formation of 1,5-PeO.

To further gain detailed information on the possible reaction mechanism during the hydrogen ring-opening process, in-situ DRIFT experiments on T_{450} catalyst was performed under H_2. The dynamic changes of functional groups in the reactant were monitored and identified at different experimental temperatures. As for gas FOL, the strong peaks located at 3358, 1069, 1145, and 1009 cm^{-1} are ascribed to –OH vibration, C-OH vibration, v_{as}(C-O-C), and v_s(C-O-C) in FOL, respectively [12] (Fig. S11). With the inflow of hydrogen and increase of temperature, three new peaks appeared at 3000–3600 (v(-OH)), 2923 (v_{as}(-CH_2-)), and 2869 cm^{-1} (v_s(-CH_2-)), and the intensity of these peaks increased with gradually enhanced temperature, indicating the formation of hydroxyl and methylene. Additionally, the C-O-C band at 1147 and 1006 cm^{-1} became negative compared with the baseline, indicating the adsorption of C-O-C at the initial heating stage (Fig. 6a).[31] However, as the temperature increased, new peaks at 1151 and 1025 cm^{-1} were observed with enhanced intensity, resulting from the formation process of the C-O bond. Furthermore, the enhanced signals at 1504 and 757 cm^{-1} corresponded to the formation of –$(CH_2)_n$- [30,32], further confirming the occurrence of ring-opening in FOL and the formation of 1,5-PeO. In-situ DRIFT results confirm that the alcoholic hydroxyl and the O atom in the furan ring are all adsorbed during the reaction, which is favorable for the ring-opening process of FOL.

The evolution of DRIFT spectra using 2-MF is similar to that of FOL (Fig. 6b). The formation of bands at 3000–3600 (v(-OH)), 2917 (v_{as}(-CH_2-)), and 2855 cm^{-1} (v_s(-CH_2-)) indicating the formation of hydroxyl and methylene, and the strengthened peaks at 1151 and 1014 cm^{-1} suggesting the appearance of C-O bond with the increase of temperature under hydrogenous atmosphere. The enhanced signals at 1460 and 746 cm^{-1} further confirmed the formation of –$(CH_2)_n$-, implying the occurrence of ring opening reaction. The hydrogenation products of 2-MF using T_{450} is n-pentanol, 2-pentanol and 2-THMF (Fig. S12a), and the selectivity of 2-pentanol is higher than n-pentanol. These results confirmed the ring opening reaction could occur without alcoholic hydroxyl, and the cleavage of C_5-O_1 was preferential due to the steric hindrance of methyl. This conclusion further proven that the ring opening process is partially relied on the adsorption of O in furan ring, and the adsorption of alcoholic hydroxyl is helpful for activating the C_2-O_1 bond, enhancing the selectivity of 1,5-PeO.

3.6. DFT calculations and reaction pathways

To further study the reaction mechanism during the ring-opening reaction, the DFT calculations were performed to uncover the correlation between the adsorption configuration of substrates and catalytic selectivity. To investigate the H_2 dissociation on the surface of T_{450} catalyst, the energy values for dissociative H_2 adsorption on Co (111), CoO (111), and O_v-CoO (111) surfaces were determined (Fig. 7a), and these surfaces are decided by HR-TEM and XRD analysis. The adsorption energy for H_2 on Co (111) surface (−0.48 eV) is considerably higher than those on CoO (111) (−0.37 eV) and O_v-CoO (111) (−0.17 eV) surfaces, indicating the H_2 molecules more tend to adsorb on Co (111) surface. The lower activation energy barriers required for H_2 dissociation on Co (111) further confirms that Co (111) is also more favorable for the dissociation of H_2 to H atoms. Therefore, the adsorption and dissociation of H_2 were thermodynamically favored on the Co^0 surface.

The adsorption sites and adsorption configurations of FOL on Co (111), CoO (111), and O_v-CoO (111) surfaces were further revealed by DFT calculations (Fig. 7b, c, d). On the Co (111) and pristine CoO (111) surfaces, FOL is preferentially adsorbed on the surface Co atoms or $Co^{\delta+}$ atom with a vertical or slightly tilted geometry through η1–(O)–alcoholic configuration. While on the surface of O_v-CoO (111), the preferential adsorption configuration of FOL is through the dual O atoms of alcohol hydroxyl and furan ring in FOL molecules. The highest adsorption energy of −0.68 eV indicates that $Co^{\delta+}$ atoms next to O_v sites could form strong interactions with O atoms of FOL, which are favorable adsorption sites. To further reveal the activation of adsorption on FOL molecules, the changes in C-O bond length and C-O-C angles in adsorbed FOL with different configurations are listed in Table S3. Compared with the gas FOL, the bond length of three C-O bonds in FOL on O_v-CoO (111) surface presents an obvious change through dual O atoms configuration on $Co^{\delta+}$ atoms next to O_v sites. In addition, the distorted C-O-C angles further confirmed the activation of adsorption on $Co^{\delta+}$ atoms next to O_v sites, which is responsible for the high efficiency and selectivity for 1,5-PeO. The d-band centers of Co located on the Co-CoO interface fell between those of Co and CoO, indicating the formation of heterojunction (Fig. S13c). While the d-band centers of Co-CoO-O_v are closer to the Fermi level than those of the Co^0 contacts with pristine CoO (Co-CoO), suggesting Co-CoO-O_v sites are more active during the reaction. To

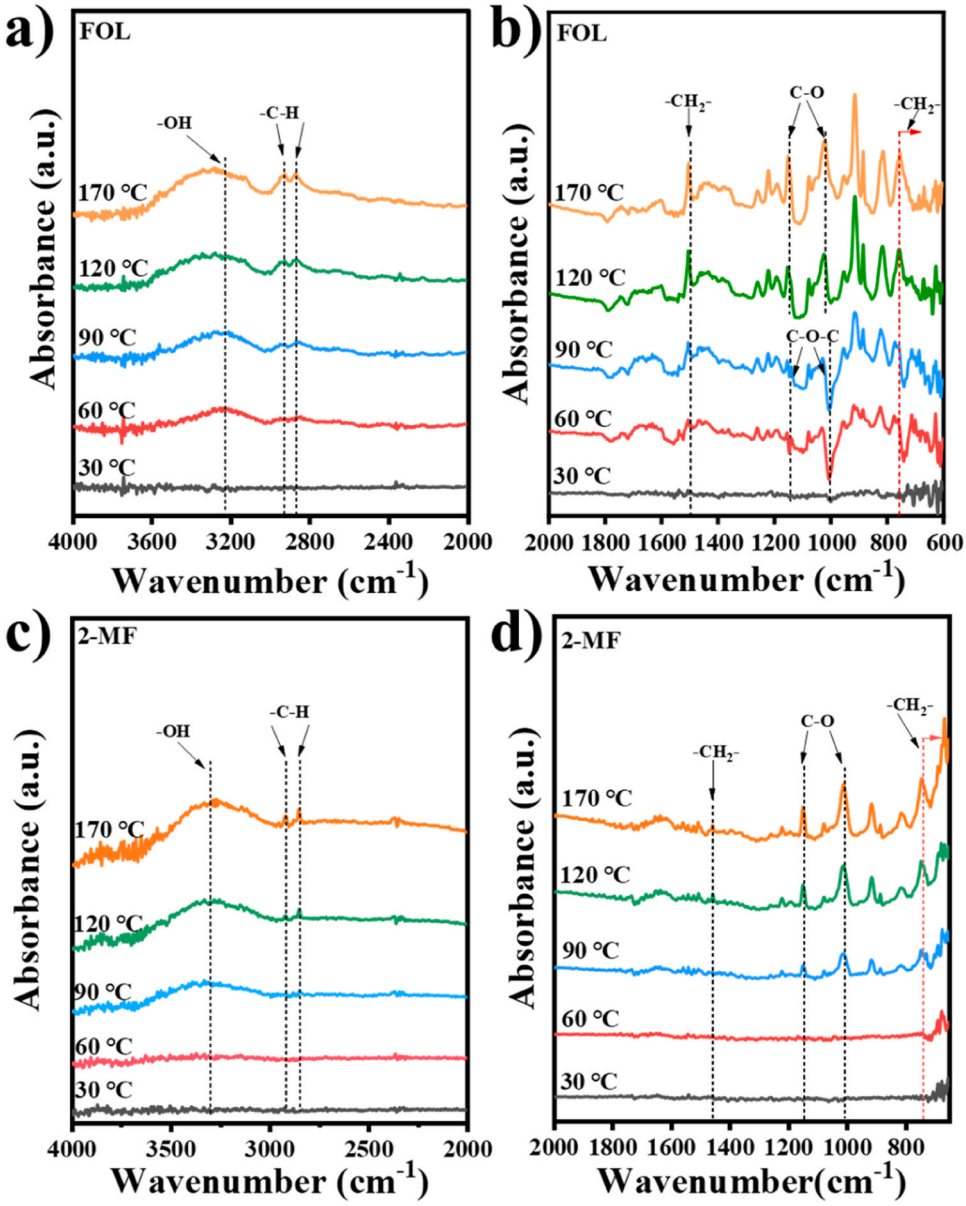

Fig. 6. In-situ DRIFT of a), b) FOL and c), d) 2-MF during hydrogenation over T_{450} catalyst.

verify the adsorption configuration of the catalyst for the reactant molecules, 2-MF without hydroxymethyl groups and 5-HMF with bis-hydroxymethyl groups were selected as reaction substrates for evaluating the hydrogenation reaction process (Fig. S12b), and the analytical results showed that both reactant molecules had ring-opening products in the product distributions, which further indicated that the FOL was adsorbed on the surface of the catalyst via the dioxygen adsorption.

To reveal the role of oxygen vacancies in the hydrogenation of FOL, the reaction routes for 1,5-PeO, 1,2-PeO, THFA, and 2-MF through dual O adsorption were investigated on pristine CoO (111) and CoO (111)-O_v interfaces with Co NPs. On the interface between Co and pristine CoO (Fig. 8a), the hydrogen atom attacks the C_2-O_1 (path 1) and C_5-O_1 (path 2) bond, resulting in the ring-opening of FOL and forms the intermediate for the final product of 1,5-PeO and 1,2-PeO. If the adsorbed H atom attacks the C═C bond in the furan ring (path 3), the furan ring becomes saturated and finally forms THFA. The attack on the C_1-O_2 bond by adsorbed H atom could lead to the cleavage and the formation of 2-MF (path 4). The hydrogenation energy barrier of four reaction routes is in the following order: 1,2-PeO (path 2) (4.29 eV) > THFA (path 3) (3.68 eV) > 2-MF (path 4) (3.21 eV) > 1,5-PeO (path 1) (2.97 eV). Hence, the formation of 1,5-PeO is thermodynamically favorable than other pathways on pristine CoO with Co. When the H atom attacked the C_2-O_1, C_5-O_1, C═C and C_1-O_2 bond of FOL on Co-CoO-O_v interfaces (Fig. 8b), the hydrogenation energy barriers are in the order of 1,2-PeO (path 2) (3.67 eV) > THFA (path 3) (3.15 eV) > 2-MF (path 4) (2.71 eV) > 1,5-PeO (path 1) (1.86 eV). Therefore, due to the activation of dual O configuration on CoO-O_v, the FOL conversion to 1,5-PeO is more favorable than on pristine CoO. The electron-enriched Co atoms adjacent to the O_v sites could adsorb the O atoms in the hydroxyl and furan ring strongly on the CoO-O_v surface, resulting in the increase of C-O bond length and disorder of the C-O-C bond. Consequently, the hydrogenation energy barrier on CoO-O_v is lower than the pristine CoO surface.

Based on the above results, a reasonable reaction pathway for the conversion of FOL to 1,5-PeO over the MOF-derived Co-CoO/C catalyst was proposed. At first, H_2 molecules are dissociative adsorbed on metallic Co sites. Next, the FOL molecule is adsorbed on the $Co^{\delta+}$ sites in the dual O configuration through O atoms from the furan ring and

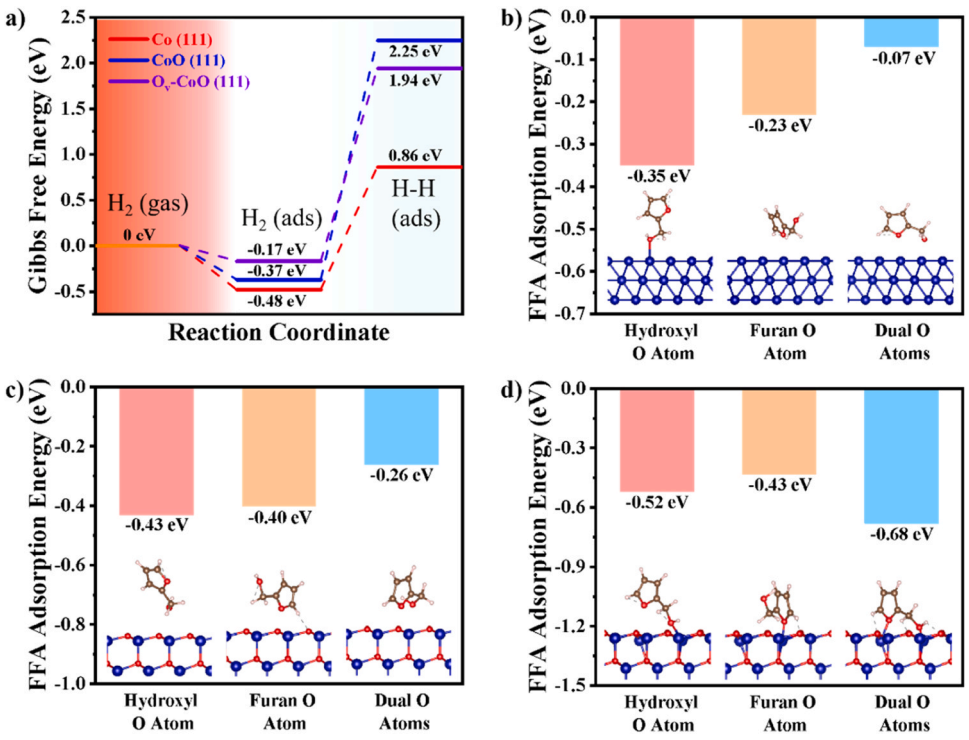

Fig. 7. a) Reaction coordinates for the dissociative adsorption of hydrogen molecules on the Co (111), CoO (111), and O_v-CoO (111) surfaces. Adsorption energies of various adsorption configurations of FOL on b) Co (111), c) CoO (111), d) O_v-CoO (111) surfaces.

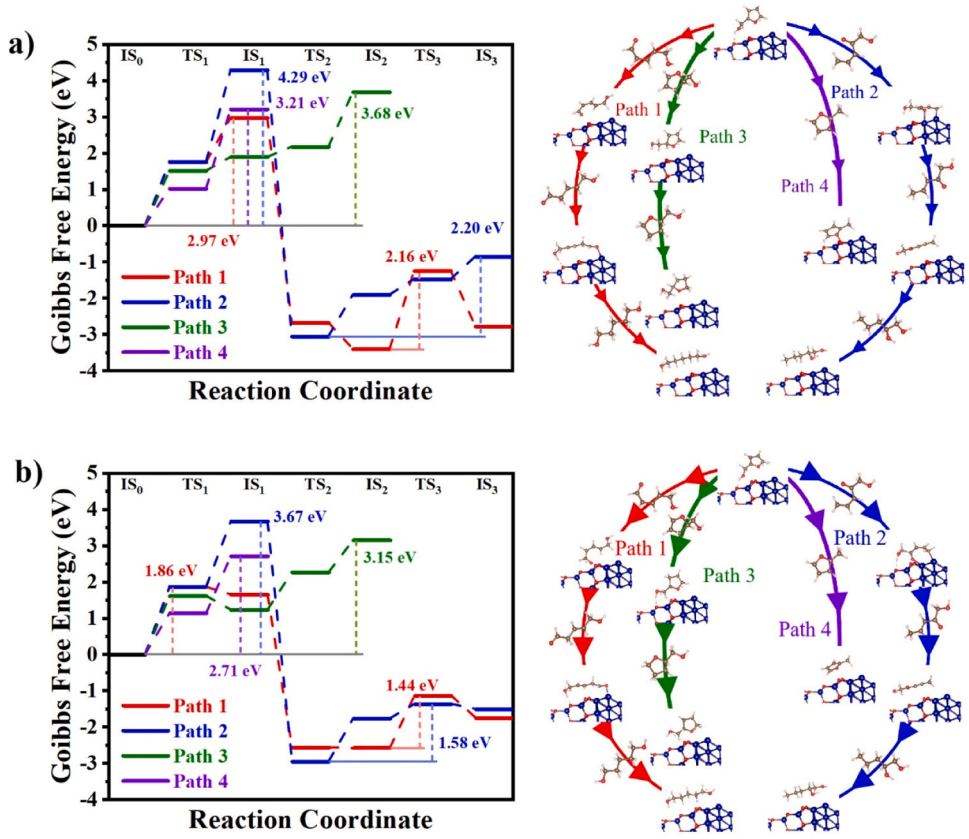

Fig. 8. a) Reaction coordinates for different reaction pathways of FOL on Co-CoO interface. b) Reaction coordinates for different reaction pathways of FOL on the Co-CoO-O_v interface.

hydroxyl. Then, dissociative H atoms attack the C_2-O_1, C_5-O_1, C═C, and C_1-O_2 bonds of adsorbed FOL. Among these competing reactions, the preferential route on the Co-CoO-O_v interface is the cleavage of the C_2-O_1 bond, resulting in the ring-open product of 1,5-PeO after further hydrogenation. The route of 1,2-PeO was significantly inhibited due to the dual O adsorption configuration, resulting in 2-MF and its corresponding derivatives becoming the main by-products.

3.7. Catalyst reusability

To investigate the stability and reusability of the T_{450} catalyst, five consecutive FOL conversation cycles were performed at optimized reaction conditions. From the first to the fifth cycle, the conversion of FOL was maintained above 90%, and the selectivity of 1,5-PeO slightly decreased from 46% to 43%, indicating the activity of T_{450} was sustained over five cycles (Fig. 9a). After the fifth cycle, the diffraction peaks of Co species were still free from XRD pattern, implying the Co NPs were not aggregated in the spent catalyst (Fig. 9b). The textural properties of spent catalysts presented difference with the fresh catalyst. The BET surface area of spent catalyst was decreased to 178 $m^2 \cdot g^{-1}$ (Fig. 9c), and the pore size distribution confirmed the decrease of surface area was mainly originated from the transformation of micropores (Fig. 9d). In addition, the morphology of the nanoflowers in the spent catalyst was maintained after cycling (Fig. S14). The Co 2p, C 1 s, N 1 s XPS spectra of the spent catalyst was similar to the fresh one (Fig. 9e, Fig. S15). While the ratio O_L in the spent catalyst was decreased slightly compared with the O 1 s spectra of the fresh catalyst, indicating partial oxides were reduced in the hydrogenous atmosphere (Fig. 9f). Therefore, the T_{450} catalyst exhibits acceptable stability during the FOL conversion to 1,5-PeO.

4. Conclusion

In conclusion, the monometallic Co-based catalyst consisting of self-derived Co-CoO_x active sites supported on carbon was synthesized from metal-organic frameworks (Co-TCPP), and were characterized thoroughly. The optimized catalyst exhibited high efficient for the conversion of FOL to 1,5-PeO with high selectivity (46%) at 170 °C, 3 MPa initial H_2 pressure for 1.5 h in ethanol. Experimental results demonstrated that the Co^{2+} coordinated with carboxyl in MOF precursor could transform into highly dispersed metallic Co^0 phases contiguous with CoO_x containing oxygen vacancy (O_v). The flower-like morphology was kept in the obtained Co-CoO_x/C materials, and there were sufficient ultrasmall Co-CoOx active sites exposed on the accessible surface. The metallic Co could boost the dissociation of H_2 molecules, and the proximate CoO_x with oxygen vacancy acted as the adsorption sites during the hydrogenolysis process of FOL. The $Co^{\delta+}$ centers adjacent to O_v sites could adsorbed the O atoms in alcoholic hydroxyl and furan ring separately. Based on the DFT results, the dual O adsorption configuration could activate the C_2-O_1 bond and furan ring, therefore the cleavage of C_2-O_1 became thermodynamically favorable than the formation of 1,2-PeO and THFA. Recyclability tests revealed that the synergic catalysis of Co-CoO_x active sites could realize the hydrogenolysis of FOL to 1,5-PeO stably. Hence, our work offers a simplified model catalytic system for revealing the reaction process from FOL to 1,5-PeO, which will be helpful for improving the production efficiency of 1,5-PeO from FOL through transition metal catalyst.

CRediT authorship contribution statement

Dai Dengfeng: Methodology, Investigation. **Xiang Taisan:** Writing – original draft, Data curation. **Liu Yunqi:** Supervision, Project administration. **Gu Xin:** Validation, Investigation. **Li Liangjun:** Supervision, Methodology. **Dai Pengcheng:** Formal analysis, Conceptualization.

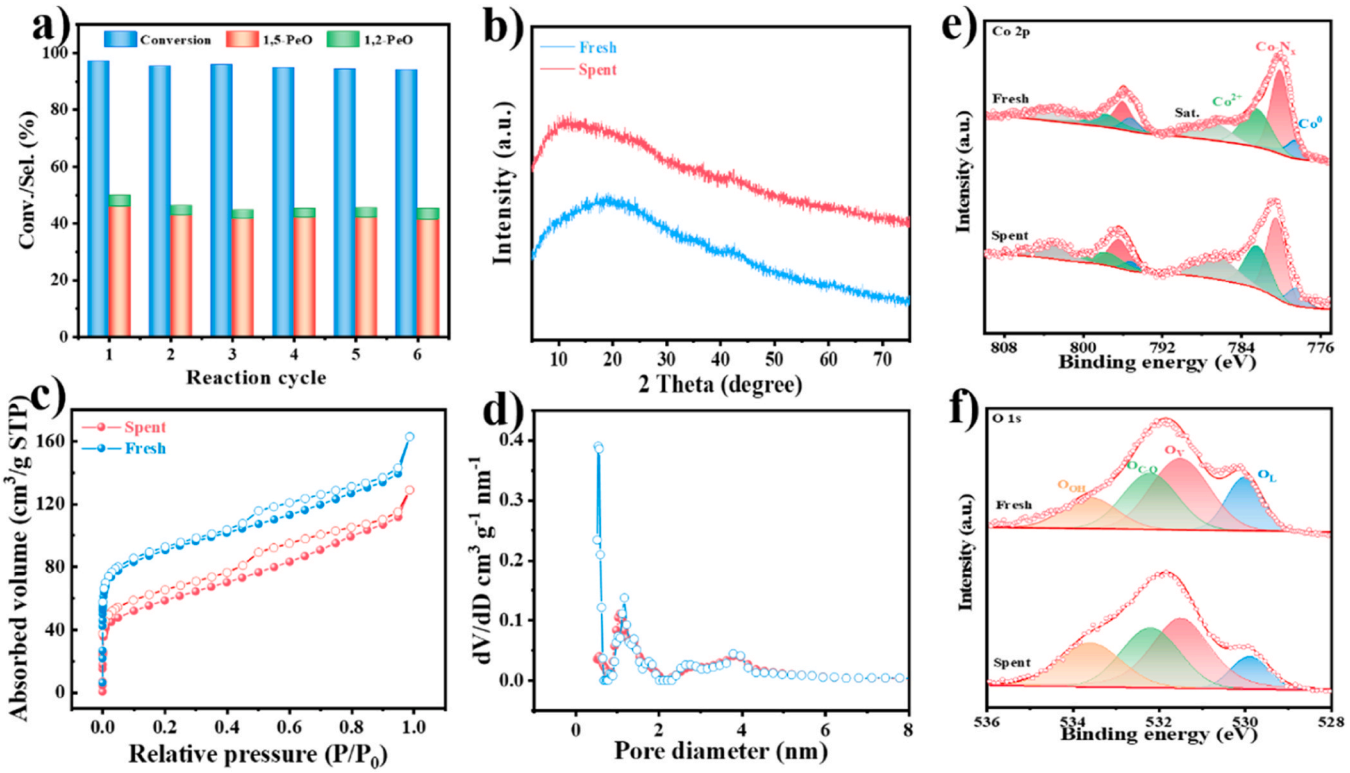

Fig. 9. a) Cycling stability of T_{450} catalyst for FOL conversion. Reaction conditions: 50 mg catalyst, 50 mL of ethanol solution dissolved in 250 mg of FOL, 170 °C, 3 Mpa H_2, and 1.5 h. b) XRD patterns, c) N_2 adsorption-desorption isotherms, d) pore size distributions, and e) Co 2p, d) O1s XPS spectra of fresh and spent T_{450} catalyst.

Feng Chao: Validation, Software. **Liu Dandan:** Writing – review & editing, Supervision, Funding acquisition. **Li Xin:** Investigation, Data curation.

Declaration of Competing Interest

The authors declare that they have no known competing financial interests or personal relationships that could have appeared to influence the work reported in this paper.

Data availability

Data will be made available on request.

Acknowledgement

This work was supported by the National Natural Science Foundation of China [grant number 22005342].

Appendix A. Supporting information

Supplementary data associated with this article can be found in the online version at doi:10.1016/j.apcatb.2024.123841.

References

[1] S. Kim, R. Xu, W. Lee, Y.T. Kang, Mass transfer performance enhancement by nanoabsorbents during CO_2 absorption process, Int. J. Heat. Mass Tran. 137 (2019) 1–11, https://doi.org/10.1016/j.ijheatmasstransfer.2019.03.098.
[2] D.M. Alonso, S.G. Wettstein, J.A. Dumesic, Bimetallic catalysts for upgrading of biomass to fuels and chemicals, Chem. Soc. Rev. 41 (2012) 8075–8098, https://doi.org/10.1039/c2cs35188a.
[3] R. Mariscal, P. Maireles-Torres, M. Ojeda, I. Sádaba, M. López Granados, Furfural: a renewable and versatile platform molecule for the synthesis of chemicals and fuels, Energ. Environ. Sci. 9 (2016) 1144–1189, https://doi.org/10.1039/c5ee02666k.
[4] K. Huang, Z.J. Brentzel, K.J. Barnett, J.A. Dumesic, G.W. Huber, C.T. Maravelias, Conversion of Furfural to 1,5-Pentanediol: Process Synthesis and Analysis, ACS Sustain. Chem. Eng. 5 (2017) 4699–4706, https://doi.org/10.1021/acssuschemeng.7b00059.
[5] Y. Nakagawa, K. Tomishige, Total hydrogenation of furan derivatives over silica-supported Ni–Pd alloy catalyst, Catal. Commun. 12 (2010) 154–156, https://doi.org/10.1016/j.catcom.2010.09.003.
[6] H.-Y. Zheng, Y.-L. Zhu, B.-T. Teng, Z.-Q. Bai, C.-H. Zhang, H.-W. Xiang, Y.-W. Li, Towards understanding the reaction pathway in vapour phase hydrogenation of furfural to 2-methylfuran, J. Mol. Catal. A: Chem. 246 (2006) 18–23, https://doi.org/10.1016/j.molcata.2005.10.003.
[7] T.P. Sulmonetti, B. Hu, S. Lee, P.K. Agrawal, C.W. Jones, Reduced Cu–Co–Al Mixed Metal Oxides for the Ring-Opening of Furfuryl Alcohol to Produce Renewable Diols, ACS Sustain. Chem. Eng. 5 (2017) 8959–8969, https://doi.org/10.1021/acssuschemeng.7b01769.
[8] Z. Wang, X. Wang, C. Zhang, Y. Yang, L. Zhou, H. Cheng, F. Zhao, Selective hydrogenolysis of tetrahydrofurfuryl alcohol to 1,5-pentanediol over PrOx promoted Ni catalysts, Catal. Today 402 (2022) 79–87, https://doi.org/10.1016/j.cattod.2022.03.008.
[9] B. Kuang, Q. Zhang, Y. Fang, Y. Bai, S. Qiu, P. Wu, Y. Qin, T. Wang, Ring Opening of Cyclic Ether for Selective Synthesis of Renewable 1,5-Pentanediol over Pt/WO_3@SiO_2 Catalysts, Ind. Eng. Chem. Res. 59 (2020) 9372–9381, https://doi.org/10.1021/acs.iecr.9b06790.
[10] S. Koso, N. Ueda, Y. Shinmi, K. Okumura, T. Kizuka, K. Tomishige, Promoting effect of Mo on the hydrogenolysis of tetrahydrofurfuryl alcohol to 1,5-pentanediol over Rh/SiO_2, J. Catal. 267 (2009) 89–92, https://doi.org/10.1016/j.jcat.2009.07.010.
[11] S. Koso, H. Watanabe, K. Okumura, Y. Nakagawa, K. Tomishige, Comparative study of Rh–MoOx and Rh–ReOx supported on SiO2 for the hydrogenolysis of ethers and polyols, Appl. Catal. B: Environ. 111-112 (2012) 27–37, https://doi.org/10.1016/j.apcatb.2011.09.015.
[12] Y. Zhu, B. Li, C. Zhao, Cu nanoparticles supported on core–shell MgO-La_2O_3 catalyzed hydrogenolysis of furfuryl alcohol to pentanediol, J. Catal. 410 (2022) 42–53, https://doi.org/10.1016/j.jcat.2022.04.018.
[13] H. Liu, Z. Huang, H. Kang, C. Xia, J. Chen, Selective hydrogenolysis of biomass-derived furfuryl alcohol into 1,2- and 1,5-pentanediol over highly dispersed Cu-Al_2O_3 catalysts, Chin. J. Catal. 37 (2016) 700–710, https://doi.org/10.1016/s1872-2067(15)61080-4.
[14] H.W. Wijaya, T. Kojima, T. Hara, N. Ichikuni, S. Shimazu, Synthesis of 1,5-Pentanediol by Hydrogenolysis of Furfuryl Alcohol over Ni-Y_2O_3 Composite Catalyst, ChemCatChem 9 (2017) 2869–2874, https://doi.org/10.1002/cctc.201700066.
[15] Y. Shao, M. Guo, J. Wang, K. Sun, L. Zhang, S. Zhang, G. Hu, L. Xu, X. Yuan, X. Hu, Selective Conversion of Furfural into Diols over Co-Based Catalysts: Importance of the Coordination of Hydrogenation Sites and Basic Sites, Ind. Eng. Chem. Res. 60 (2021) 10393–10406, https://doi.org/10.1021/acs.iecr.1c01051.
[16] R.G. Kurniawan, N. Karanwal, J. Park, D. Verma, S.K. Kwak, S.K. Kim, J. Kim, Direct conversion of furfural to 1,5-pentanediol over a nickel–cobalt oxide–alumina trimetallic catalyst, Appl. Catal. B: Environ. 320 (2023), https://doi.org/10.1016/j.apcatb.2022.121971.
[17] J. Peng, D. Zhang, Y. Wu, H. Wang, X. Tian, M. Ding, Selectivity control of furfuryl alcohol upgrading to 1,5-pentanediol over hydrotalcite-derived Ni-Co-Al catalyst, Fuel 332 (2023), https://doi.org/10.1016/j.fuel.2022.126261.
[18] Q. Wang, D. Astruc, State of the Art and Prospects in Metal-Organic Framework (MOF)-Based and MOF-Derived Nanocatalysis, Chem. Rev. 120 (2020) 1438–1511, https://doi.org/10.1021/acs.chemrev.9b00223.
[19] S. Zhao, Y. Long, Y. Su, S. Wang, Z. Zhang, X. Zhang, Cobalt-Enhanced Mass Transfer and Catalytic Production of Sulfate Radicals in MOF-Derived CeO_2 • Co_3O_4 Nanoflowers for Efficient Degradation of Antibiotics, Small 17 (2021), https://doi.org/10.1002/smll.202101393.
[20] R. Rahimi, S. Shariatinia, S. Zargari, M. Yaghoubi Berijani, A. Ghaffarinejad, Z. S. Shojaie, Synthesis, characterization, and photocurrent generation of a new nanocomposite based Cu–TCPP MOF and ZnO nanorod, RSC Adv. 5 (2015) 46624–46631, https://doi.org/10.1039/c5ra02882e.
[21] L. Wang, S. Duan, P. Jin, H. She, J. Huang, Z. Lei, T. Zhang, Q. Wang, Anchored Cu (II) tetra(4-carboxylphenyl)porphyrin to P25 (TiO_2) for efficient photocatalytic ability in CO_2 reduction, Appl. Catal. B: Environ. 239 (2018) 599–608, https://doi.org/10.1016/j.apcatb.2018.08.007.
[22] V. Ranaware, R.G. Kurniawan, D. Verma, S.K. Kwak, B.C. Ryu, J.W. Kang, J. Kim, Solvent-mediated selectivity control of furfural hydrogenation over a N-doped carbon-nanotube-supported Co/CoO_x catalyst, Appl. Catal. B: Environ. 318 (2022), https://doi.org/10.1016/j.apcatb.2022.121838.
[23] Y. Wu, L. Wang, L. Chen, Y. Li, K. Shen, Morphology-Engineering Construction of Anti-Aggregated Co/N-Doped Hollow Carbon from Metal-Organic Frameworks for Efficient Biomass Upgrading, Small 19 (2023) e2207689, https://doi.org/10.1002/smll.202207689.
[24] H. Li, M. Zhang, W. Zhou, J. Duan, W. Jin, Ultrathin 2D catalysts with N-coordinated single Co atom outside Co cluster for highly efficient Zn-air battery, Chem. Eng. J. 421 (2021), https://doi.org/10.1016/j.cej.2021.129719.
[25] G. Wang, X. Nie, X. Ji, X. Quan, S. Chen, H. Wang, H. Yu, X. Guo, Enhanced heterogeneous activation of peroxymonosulfate by Co and N codoped porous carbon for degradation of organic pollutants: the synergism between Co and N, Environ. Sci. Nano 6 (2019) 399–410, https://doi.org/10.1039/c8en01231h.
[26] L. Jiao, G. Wan, R. Zhang, H. Zhou, S.H. Yu, H.L. Jiang, From Metal-Organic Frameworks to Single-Atom Fe Implanted N-doped Porous Carbons: Efficient Oxygen Reduction in Both Alkaline and Acidic Media, Angew. Chem. Int. Ed. 57 (2018) 8525–8529, https://doi.org/10.1002/anie.201803262.
[27] Y. Yao, C. Wang, Y. Yang, S. Zhang, X. Yan, C. Xiao, Y. Zhou, Z. Zhu, J. Qi, X. Sun, J. Li, Mn-Co dual sites relay activation of peroxymonosulfate for accelerated decontamination, Appl. Catal. B Environ. 330 (2023), https://doi.org/10.1016/j.apcatb.2023.122656.
[28] S. Xiang, L. Dong, Z.Q. Wang, X. Han, L.L. Daemen, J. Li, Y. Cheng, Y. Guo, X. Liu, Y. Hu, A.J. Ramirez-Cuesta, S. Yang, X.Q. Gong, Y. Wang, A unique Co@CoO catalyst for hydrogenolysis of biomass-derived 5-hydroxymethylfurfural to 2,5-dimethylfuran, Nat. Commun. 13 (2022) 3657, https://doi.org/10.1038/s41467-022-31362-9.
[29] L. Pino, C. Italiano, A. Vita, M. Laganà, V. Recupero, $Ce_{0.70}La_{0.20}Ni_{0.10}O_2$-δ catalyst for methane dry reforming: Influence of reduction temperature on the catalytic activity and stability, Appl. Catal. B Environ. 218 (2017) 779–792, https://doi.org/10.1016/j.apcatb.2017.06.080.
[30] Y. Shao, J. Wang, H. Du, K. Sun, Z. Zhang, L. Zhang, Q. Li, S. Zhang, Q. Liu, X. Hu, Importance of Magnesium in Cu-Based Catalysts for Selective Conversion of Biomass-Derived Furan Compounds to Diols, ACS Sustain. Chem. Eng. 8 (2020) 5217–5228, https://doi.org/10.1021/acssuschemeng.9b07841.
[31] L. Huang, L. Wang, Z. Zhang, X. Guo, X. Zhang, J.M. Chabu, P. Liu, F. Tang, Understanding the promotional effects of trace doped Zn in Co/NC for efficient one-pot catalytic conversion of furfural to 2-methyl-tetrahydrofuran, J. Energy Chem. 71 (2022) 225–233, https://doi.org/10.1016/j.jechem.2022.03.031.
[32] X. Meng, Y. Yang, L. Chen, M. Xu, X. Zhang, M. Wei, A Control over Hydrogenation Selectivity of Furfural via Tuning Exposed Facet of Ni Catalysts, ACS Catal. 9 (2019) 4226–4235, https://doi.org/10.1021/acscatal.9b00238.